Surface Properties of ZnS Nanoparticles: A Combined DFT and Experimental Study

Elena Balantseva,Gloria Berlier,Bruno Camino,Martina Lessio,Anna Maria Ferrari
Surface Properties of ZnS Nanoparticles: A Combined DFT and Experimental Study
JOURNAL OF PHYSICAL CHEMISTRY. C, NANOMATERIALS AND INTERFACES (2014) 118
DOI: 10.1021/jp507963y

Surface properties of ZnS nanoparticles: a combined DFT and experimental study

Elena Balensteva,[1] Gloria Berlier,[1] Bruno Camino,[2] Martina Lessio,[3] Anna Maria Ferrari[1,1]

[1]*Università di Torino, Dipartimento di Chimica and NIS (Nanostructured Interfaces and Surfaces) Centre, Via P. Giuria 7, 10125 Torino, Italy*
[2]*Department of Chemistry, Imperial College London, South Kensington London SW7 2AZ*
[3]*Princeton University Department of Mechanical and Aerospace Engineering D404A Engineering Quadrangle Princeton, NJ 08544*

Abstract

Carbon monoxide adsorption on nanosize ZnS has been investigated by FTIR spectroscopy and periodic DFT calculations. FTIR experiments show that CO adsorption on the zinc sulfide nanoparticles gives rise to a single main ν(CO) band indicating that the majority of the exposed sites are on the same surface. Computed adsorption energies (-0.244/-0.207 eV for the low and high coverage, respectively) and stretching frequencies (2182/2172 cm^{-1}) of CO adsorbed at the most stable (110) ZnS surface are in excellent agreement with observations (ν(CO)=2190/2168 cm^{-1}). CO is weakly bound to the Zn^{2+} Lewis acid surface site mainly through electrostatic interaction and a small contribution from σ donation. The strength of surface Lewis sites in ZnS is lower with respect to ZnO.

Keywords: Infrared spectroscopy; Density functional theory; Carbon monoxide; zinc sulfide nanoparticles

[1] Anna Maria Ferrari
Dipartimento di Chimica
Università di Torino
Via P. Giuria 5 10125 Torino Italy
Email: anna.ferrari@unito.it

1. Introduction

ZnS is one of the most important materials in the electronic industry with a wide range of applications. These includes photonic, nonlinear optical devices, light-emitting diodes, flat panel displays, infrared windows, field emitters, sensors, and lasers.[1-3] The key role of morphology, size, and chemical composition in engineering the electronic fine structure of semiconductors was pointed out in many papers.[4-8]. Among direct II–VI semiconductors zinc sulfide (ZnS) is a well-known wide band gap material, with room temperature energy gap (E_g) around 3.7 eV. Cubic zinc blende (sphalerite) and hexagonal (wurtzite) are the two ZnS polymorphs, with slightly different E_g (3.72 vs 3.77 eV, respectively). ZnS has been prepared and studied in many structures and morphologies, such as bulk materials, thin films, wires, nano belts and nano particles, depending on the synthesis procedure and desired application.[9-11]

Growing interest in the field is currently related to the study of ZnS-based materials, prepared by doping or solid solution formation with transition metal ions or narrow band gap semiconductors, respectively.[12-18] The former class of materials (doped with Mn, Cu, Ni, etc.) were mainly proposed to develop specific luminescence properties for applications in solar cells, biomedical diagnosis, light-emitting diodes (LEDs) and so on.[12,14,17-19] Another important application, where ZnS solid solutions with InS_2, AgS and/or CuS showed promising activity, is the photocatalytic water splitting in the presence of sulfite as sacrificial agents, as an eco-friendly alternative to toxic CdS.[13,16,20]

Notwithstanding the intense research activity on the synthesis and properties of nanostructured ZnS materials, very little information is available about their surface structure. As recently pointed out by Gilbert et al., surface chemistry can have an important role in controlling ZnS crystal growth.[21] This includes the presence of defects or disorder and of surface ligands or adsorbed species, which can determine important properties, including optical absorption threshold position and photoluminescence efficiency.[21-24] Furthermore, a description of the surface from an atomic point of view could be crucial for an understanding of photocatalytic processes.

Very few techniques are available to study the surface properties of nanoparticles, so that often indirect methods are necessary. Among these, the employ of *in situ* infrared spectroscopy is a very powerful tool,[25] especially when coupled to theoretical modeling allowing the calculation of energy, structure and vibrational frequencies of simple molecules weakly interacting with the surface.[26]

The literature concerning *in situ* infrared studies of sulfide materials is quite limited with respect to oxides. Some works were reported about the surface properties of unsupported or supported MoS_2, an increasingly studied catalyst for hydrodesulfidation.[27-30] On the contrary, only

few reports can be found about the surface chemistry of ZnS. Namely, *in situ* infrared was employed to characterize a ZnS evaporated film[31] or two low specific surface area commercial wurtzite and wurtzite/sphalerite samples.[32] The role of water adsorption on ZnS nanoparticles growth was also followed.[21] More commonly, infrared spectroscopy has been employed to study ZnS based materials with particular attention to the presence of additives,[33] surface capping agents[34] or chemicals adsorbed during the synthesis.[35] Far-infrared spectra (often coupled to Raman) have been instead used for structural characterization of various sulfides, giving information on the presence of mixed stacking.[36,37]

One of the reasons for this lack of information on ZnS surface could be related to the intrinsic difficulties in handling this class of materials. In the case of oxides *in situ* surface studies are usually carried out on cleaned surfaces, obtained by removing species adsorbed from the atmosphere or residual synthetic reactants by calcination/oxidation treatments in flow or static conditions. This is not straightforward for sulfides; for instance it is well known that calcination at temperatures as high as 773 K causes the transformation of ZnS to ZnO.[36,38,39] Even if oxidation is carried out in controlled conditions, by avoiding the complete ZnS/ZnO phase transition, treatment with oxygen or water vapor were shown to cause the formation of surface sulfate (SO_4^{2-}) and sulfite (SO_3^{2-}) species.[40]

On the other hand, nanostructuration is often obtained by employing capping agents, which should stop the particle growth. This clearly influences the structure of metal or sulfur surface atoms, but can also have important effects on the material optical properties,[34,41] shape and morphology[42] or crystalline phase.[43] Another interesting and easy synthetic method for ZnS nanoparticles is based on the use of thioacetamide in the presence of acetate anions;[44] both chemicals can remain absorbed on the surface of the final product unless careful washing is carried out.[35,37,44] These examples show how surface studies on nanoparticles can be seriously affected by the presence of adsorbed species, since the procedures employed to clean the surface can affect the particle stability and morphology. Another interesting aspect in nanostructured metal chalcogenides (sulfides, selenides and tellurides) is the stoichiometry of the surface. For instance, NiS and CoS nanoparticles inside zeolites were reported to be poor in sulfur,[45] while the Zn/S ratio in ZnS thin films was found to be dependent upon the film thickness and employed complexing agent.[46] On the basis of low temperature Extended X-Ray Adsorption Fine Structure (EXAFS) experiments, some of us found out that the Zn first shell coordination number was not affected by nanostructuration, on samples prepared by the thioacetamide method.[44] This suggests a 1:1 Zn:S stoichiometry on the bulk and surface of this kind of materials.

From the theoretical point of view, the crystal growth of ZnS nanoclusters was extensively studied in the group of Prof. Catlow.[47-51] These works were mainly devoted to the prediction of crystal structure and shape/morphology at the very early nucleation steps.[48,51] Other works were devoted to the prediction of ZnS-based mesostructures.[52] The electronic properties of nanosized ZnS were also extensively studied by time-dependent density functional theory (TD-DFT).[53-58] To the best of our knowledge very few reports were instead reported on the description of ZnS surfaces and on their reactivity with small molecules.[59]

This paper reports the results obtained by *in situ* infrared spectroscopy on a nanostructured ZnS sample prepared by a simple chemical precipitation method based on the use of thioacetamide. The aim of the work is the description of the effect of nanostructuration on the properties of ZnS surface sites, by employing the CO molecular probe on samples outgassed at increasing temperature. The experiments were supported by the theoretical modeling of the properties (adsorption energies and vibrational features) of CO adsorbed at the most stable (110) ZnS surface.

2. Experimental Section

2.1. Synthesis

Thioacetamide (CH_3CSNH_2, TAA) was purchased from Sigma Aldrich; analytical grade zinc acetate ($Zn(CH_3COO)_2 \cdot 2H_2O$, ZnAc) from Baker Analyzed ACS Reagent; methanol and ethanol from Carlo Erba reagents. Bulk ZnS (powder, <10 μm, 99.99%) was purchased from Sigma Aldrich. All the chemical and solvents were used as received without further purification.

In a typical procedure TAA and ZnAc were dissolved separately in ethanol/methanol 1/1 mixture at 313 K, to give 0.2 M equimolar solutions. The TAA solution was then slowly added to the ZnAc one under continuous stirring. The resulting mixture (50 ml total volume) was left under stirring for 6 h. Afterwards the resulting white powder was separated by centrifugation (4000 rpm), and washed first with the alcohol mixture and then trice with hot distilled water. The cleaned product was dried for about 3 h in oven at 353 K. The obtained samples were carefully ground before characterization.

2.2. Characterization

Powder X ray diffraction (XRD) patterns were measured with PW3050/60 X'Pert PRO MPD diffractometer (Panalytical) working in Bragg–Brentano geometry using Cu Kα radiation (λ =1.5406 Å) and operated at 45kV, 40mA with a scan speed of 0.01° min^{-1}. The crystallite size was calculated according to the Scherrer's equation, $L=k\lambda/(\beta \cos\theta)$ where L is the crystal size, λ the X-ray wavelength, β the broadening of the diffraction peak and θ the diffraction angle.[47] High

Resolution Transmission Electron Microscopy (HRTEM) measurements were performed on JEM 3010-UHR microscope (JEOL Ltd.) operating at 300 kV. For the measurements ZnS powder was dispersed on a copper grid coated with a perforated carbon film.

Gasvolumetric nitrogen adsorption/desorption isotherms were measured at liquid nitrogen temperature (LNT) with ASAP 2020 physisorption analyzer (Micromeritics). Prior to analyses, samples were evacuated at 423 K over 2h. The specific surface area SSA was calculated by the Brunauer-Emmett-Teller (BET) method in the p/p_0 range from 0.05 to 0.2.[60] This is based on the equation:

$$\frac{p}{V(p_0 - p)} = \frac{1}{V_m c} + \frac{c-1}{V_m c}\frac{p}{p_0}$$

where V is the quantity of gas adsorbed at pressure p, p_0 is the saturation pressure of the gas, V_m is the amount of gas adsorbed at the monolayer formation. The value of c on simplest terms is:

$$c \propto \exp\frac{q_1 - q_L}{RT}$$

where q_1 is the heat of adsorption of the first layer, q_L the heat of liquefaction of the adsorptive, R the gas constant and T the absolute temperature.[61]

The average pore size and volume were calculated on the adsorption branch of the isotherms according to the Barrett-Joyner-Halenda (BJH) method.[61,62] This is based on an iterative process where pore size distributions are calculated upon an imaginary emptying of condensed adsorptive in the pores in a stepwise manner as the relative pressure is likewise decreased. [63] The calculation is based on the Kelvin equation assuming capillary condensation of the adsorbed phase inside the pores:

$$\frac{p^*}{p_0} = \exp\left[-\frac{2\gamma\bar{V}\cos\varphi}{r_m RT}\right]$$

The critical condensation pressure p^* in Kelvin equation is related to the mean radius of the curvature of liquid meniscus r_m, with γ being the liquid surface tension, ν the molar volume of the condensed adsorptive, θ the contact angle between the solid and condensed phase. The average pore radius r is obtained by substituting (r-t) for r_m, where t is the thickness of the adsorbed layer remaining in the pore walls, calculated with the thickness equation from Faas and Halsey:[61]

$$t = 3.54\left(\frac{-5}{\ln p/p_0}\right)^{0.333}$$

Fourier transform infrared (FTIR) spectra were recorded with an IFS66 spectrophotometer (Bruker) equipped with a DTGS detector, working with resolution of 4 cm^{-1} over 32 scans. Samples were in the form of self-supporting pellets suitable for transmission infrared experiments and were placed in a quartz cell equipped with KBr windows, designed for low temperature studies in vacuum and controlled atmosphere. Before infrared analysis the samples were evacuated at the desired temperature (from 673 to 973 K) for 1 hour. CO adsorption experiments were carried out at LNT (110 K nominal temperature) by contacting the outgassed ZnS pellet with increasing equilibrium pressure of CO (p_{CO}). Once reached 30 mbar p_{CO} was stepwise decreased (residual pressure under dynamic outgassing $1 \cdot 10^{-3}$ mbar). The reported CO spectra were background subtracted by employing as a reference the ZnS spectrum measured immediately before CO dosage. For simplicity only the spectra measured in the $2\text{-}1 \cdot 10^{-3}$ mbar range are reported, to avoid the contribution of physisorbed (liquid-like) CO.

2.3. Computational details

Results presented are obtained with periodic CRYSTAL09 code,[64] using the hybrid PBE0 DFT functional.[65] Indeed, a recent report concerning the interaction of CO with TiO_2 nanocrystals has demonstrated that the selected functional is able to provide a realistic description of the energetic and the vibrational properties of the surface adsorbates.[26]

In the CRYSTAL code, the level of accuracy in evaluating the Coulomb and the exchange series is controlled by five parameters[64] for which 10^{-7}, 10^{-7}, 10^{-7}, 10^{-7}, 10^{-18} values have been used for all calculations. The convergence threshold for SCF energy was set to 10^{-9} Ha. The reciprocal space was sampled according to a regular sublattice determined by the shrinking factor IS.[64] A value of IS=8 has been adopted which corresponds to 34 independent k-points in the irreducible part of the Brillouin zone.

The surfaces of crystals were modeled with bidimensional slabs characterized by two infinite dimensions (x, y) and a finite thickness. In particular the (110) surface has been investigated by employing a 9 ZnS-layers slab that corresponds to a thickness of about 20 Å. Stoichiometric ZnS slabs (Zn/S ratio equal to 1/1) were considered, in agreement with the experimental and theoretical reports.[44,47-50]

Different CO coverages were considered and modeled by employing supercells of appropriate size; we define the coverage θ as the ratio between the number of adsorbed molecules and the number of surface three-coordinated Zn sites. For θ=0.5 a 2x1 supercell has been built up, whereas θ=1 corresponds to the 1*x*1 cell.

Basis sets of least of triple-zed TZ quality for the valence electrons have been employed: a 511111-411-11 [6s3p2d] basis set for C and O,[66] and the relativistic Steven-Krauss small core RECP with a 4211-41 [4sp2d] basis set for valence electrons for Zn atoms[67] combined to a 8-6311-1 [1s-4sp-1d] for S in ZnS.[68]

The geometry optimization has been performed relaxing all the atoms in the cell and keeping fixed the lattice parameters at the bulk values. All the symmetry constraints have been removed. Adsorbate frequencies have been computed at the Γ point, within the harmonic approximation, by diagonalizing the mass-weighted Hessian matrix only for the adsorbate fragment, once checked that its vibrational modes are not coupled with other crystal phonons.

The Adsorption Energy (ΔE_{ads}) per molecule is calculated as:

$$\Delta E_{ads} = \frac{E_a - nE_m - E_{slab}}{n}$$

where E_m is the Energy of the optimized isolated molecule, E_{slab} is the energy of the optimized isolated slab modelling the 110 surface and n is the number of molecules per cell. The basis set superposition error BSSE has been computed and results are corrected according to the counterpoise method.[69]

For a stoichiometric surface, the Surface Energy (E_S) is calculated as:

$$E_S = \frac{E_{slab} - nE_{bulk}}{2A}$$

where E_{slab} is the energy of an n-layered 2D slab used to model the material that exposes the surface of interest, E_{bulk} is the energy of the bulk material and A is the area of the 2D surface cell. The factor 1/2 accounts for the existence of two limiting surfaces. E_S is then the energy per unit area required to form the surface from the bulk and it is reported in J/m^2.

3. Results and Discussion

3.1 General properties.

The XRD pattern of the ZnS samples was measured after thermal activation in vacuum at increasing temperature (Figure 1). This was carried out to check the structural changes induced by the thermal activation, necessary to clean the surface prior to *in situ* infrared studies (see below). Three well-defined and broad diffraction peaks, corresponding to the (111), (220) and (311) lattice planes of ZnS cubic sphalerite structure (JCPDS 010800020) are present in the samples outgassed

at 673 and 773 K, similarly to what was observed for the as prepared sample (not reported). Only after thermal activation in vacuum at 973 K (curve c in Figure 1), extra peaks related to ZnO (hexagonal phase, JCPDS 000361451) are formed, together with peaks related to the ZnS hexagonal wurtzite structure (JCPDS 000361450). Notwithstanding this transformation, the ZnS cubic phase still represents the major fraction of the sample (70-80 % as a rough approximation based on the relative intensities of the XRD peaks).

We acknowledge the fact that a partial ZnS/ZnO transformation was already observed at 673 K when the thermal activation was carried out in air or in nitrogen/oxygen flow (not reported), in agreement with literature reports.[36,38,39] The formation of a small amount of ZnO in vacuum after activation at 973 K could be explained by high temperature reaction of ZnS with adsorbed species (*i.e.* water and acetates from the synthesis). As for the ZnS phases, it is well known that the cubic form is the thermodynamically stable at low temperature, while the hexagonal one (wurtzite) is usually formed at around 1300 K.[70,71] The lower temperature at which the transition phase took place in this work is related to the nanometer size of the prepared particles (see below), in agreement with literature data and theoretical predictions.[72,73]

The full width at half maximum (FWHM) of the reported (111) peaks was employed to calculate the crystallite minimum size by employing the Scherrer equation, as summarized in Table 1. These data clearly show a gradual increase of particle size as a function of activation temperature, as a consequence of particle agglomeration (see also Figure S1 in the Supplementary Information).

Interestingly, a consistent shift in the peaks position is observed in the patterns reported in Figure 1. The main (111) peak of the sample activated at 973 K (curve c), is slightly higher with respect to that of the reference bulk cubic ZnS (data not reported and JCPDS 010800020), that is 28.62 *vs* 28.531°, respectively. The same peak is instead found at 29.16 and 29.01° in the samples activated at 773 and 673 K (curves b and a), respectively. This corresponds to a decrease in the d spacing, passing from 3.123 Å in the bulk sample, down to 3.06 Å in the sample activated at 673 K. The result is in agreement with the EXFAS analysis carried out by some of us on similar samples, showing a decrease of the Zn-S and Zn-Zn distances with particle size decrease.[44] A similar lattice contraction with respect to the bulk, indicating a compressive strain was observed for thiol-capped CdSe nanocrystals (see references therein for other examples),[74] On the contrary Rockenberger et al. showed different behavior (expansion or contraction) in CdS nanoparticles depending on the stabilizing agent.[75]

The textural properties of the samples were determined by gasvolumetric analysis, as shown in Figure S2 and summarized in Table 1. The samples could be classified as mesoporous (type IV

isotherms), with a large available volume (0.2-0.6 m^3/g) related to interparticle porosity. The SSA decreased almost linearly with activation temperature, with an opposite trend with respect to particle size (Figure S1). This was accompanied by an increase in the average pore size.

The effect of thermal activation on particle size and morphology was further investigated by TEM analysis (Figure 2). The TEM images of the sample as prepared (not reported) and after thermal activation in vacuum at 673 (Figure 2a) are similar, being characterized by dense agglomerates of spheroidal particles. The high density of the material did not allow obtaining high resolution images of single particles. To avoid this problem sonication of diluted suspensions of ZnS particles in alcohol or water was also carried out, but no differences could be observed by TEM. As a consequence, it was not possible to measure the size of a statistically relevant number of particles. The average values reported in Table 1 (measured on 20-50 particles) are thus only reported to show the trend induced by thermal treatments, which is in agreement with XRD data. Lattice fringes are visible in the TEM micrograph, indicating the crystalline nature of the particles. Fourier Transform (FT) analysis of the images resulted in a diffraction ring with average d-spacing of 3.0 Å, characteristic of the (111) peak of ZnS cubic structure (Figure S3).

Figures 2b and c show the influence on the sample size and morphology of the treatment temperature. After outgassing at 773 K (Figure 2b) the sample can still be described as a dense agglomerate of spheroidal nanoparticles (average size 6.4 ± 1.0 nm, see Table 1), but the presence of small crystalline domains is more evident, due to larger particle size and/or improved crystallinity. The main d-spacing measured on the diffraction ring of the FT is again 3.0 Å, with a small contribution of some spots at 1.8 Å, corresponding to the (220) cubic plane. After activation in vacuum at 973 K relatively large particles (35.9 ± 6.1 nm) are formed. These are mainly characterized by an ellipsoidal shape, together with smaller irregular spheroidal particles (Figure 2c). The heterogeneity in particle size and shape is in agreement with the presence of different phases, as evidenced by XRD data. This is further supported by the d-spacing measured by FT, which are mainly related to cubic ZnS ((111) and (220) planes), with a minor contribution from the hexagonal wurtzite phase ((100), (101), (102), (110) and (112)) and from hexagonal ZnO ((100) and (101)).

Finally, a commercial bulk ZnS sample was measured for comparison. A representative TEM image can be observed in Figure 2d. The sample is composed of large ellipsoidal particles, similar to those observed on the sample prepared in this work after treatment at 973 K, but more regular and homogeneous. FT analysis of the images resulted in diffractions spots suggesting the

main presence of cubic ZnS, with a fraction of the hexagonal structure, in agreement with XRD (not reported).

3.2 Surface properties: CO adsorption experiments

The surface properties of the nanostructured ZnS samples were experimentally investigated by following CO adsorption with infrared spectroscopy. The experiments were carried out at LNT (nominal temperature 110 K) by stepwise CO pressure (p_{CO}) increase and subsequent decrease. The same experiment was carried out at room temperature, but no bands related to adsorbed CO could be observed. The spectra measured upon CO desorption at LNT on the sample previously outgassed at 673 and 973 K are reported in Figure 3a and 3b, respectively.

In both panels of Figure 3 a single peak is observed, with similar maxima position at high coverage (2172-2170 cm^{-1}). On the sample activated at 673 K the peak is slightly asymmetric towards the high frequency side and broader with respect to that measured after activation at 973 K (FWHM passing from *ca* 16 to 10 cm^{-1}). In both cases a significant blue-shift is observed upon pressure decrease, but the maxima position measured at low coverage is dependent upon the sample pre-activation, in that it moves from 2191 to 2185 cm^{-1} from the sample activated at 673 K to that treated at 973 K. The same experiment was carried out after activation at 773 and 873 K. The former gave spectra undistinguishable from those of Figure 3a, while the latter showed an intermediate trend with respect to those shown in the two panels (not reported). In other words, the FWHM and band position at lower coverage, decrease almost linearly with the activation temperature. This is also accompanied by a decrease in the band intensity (compare Figures 3a and 3b), which is proportional to the amount of exposed surface sites, in agreement with the changes observed in particle size and SSA (Table 1). The same experiment carried out on a bulk ZnS sample (top curves of Figure 3b) results in a similar set of spectra, with the low coverage peak now found at 2175 cm^{-1}.

The described spectral features can be safely explained with a weak interaction of CO with Lewis acid sites, that is, with surface Zn^{2+} ions. This hypothesis is supported by comparison with literature data on ZnO. CO adsorption on ZnO microcrystals resulted in a main peak at 2190 cm^{-1} at low coverage, moving to 2168 cm^{-1} upon coverage increase. This was assigned to the adsorption on extended and regular (1010) prismatic phase, as evidenced by HRTEM measurements.[76] On the contrary, on different ZnO samples Ghiotti et al. observed a complex group of bands upon CO dosage, ranging from 2145 to 2187 cm^{-1}, testifying of the presence of different exposed surfaces.[77] In both cases CO was able to form stable adducts also at room temperature, at variance with respect to what observed in this work with ZnS.

For an interpretation of the reported data, it is worth to remind the fact that both XRD and HRTEM showed an increase in particle size and crystallinity by increasing the activation temperature. These changes correspond to a shift toward lower frequency of the vibrational mode of adsorbed CO. Indeed, the ν(CO) position (measure at low coverage) shifts from 2191 cm^{-1} in ZnS sample activated at 673 K (particle size around 5 nm), to 2185 cm^{-1} in the one activated at 973 K (particle size around 35 nm), to 2175 cm^{-1} in bulk ZnS (particle size < 10 μm). Nevertheless, the correlation between particle size and ν(CO) is not straightforward because of the larger heterogeneity in particle sizes and the lower degree of cristallinity in ZnS sample activated at temperature ≤ 773 K.

The present observations unambiguously prove, with respect to ZnO: i) the FTIR spectra show only one peak, that is, only one kind of exposed Zn^{2+} sites that therefore belong to the same surface; ii) CO does not form stable CO adducts at RT, irrespective of the activation conditions and ZnS particle size, thus indicating that the exposed active sites on ZnS show a minor Lewis acid strength with respect to those present on ZnO samples.

The observed ν(CO) shift to 2172-2170 cm^{-1} with coverage increase can be ascribed to CO dipole-dipole through space interaction (either dynamic or static).[76] This effect is hardly dependent on particle size (that is on the extent of exposed faces), in that the position of the CO peak at high coverage is very similar on the samples activated at 673 and 973 K and on bulk ZnS.

3.3 Results from DFT calculations.

Low index ZnS surfaces and namely the (110), (111) and (100) are schematically depicted in Figure 4. Their surface energy are: E_S=0.6, 1.0 and 1.7 J/m^2 for the (110), (111) and (100) surfaces, respectively. The large differences in the computed E_S is related to the geometrical structure of the exposed surfaces. Indeed according to Tasker's electrostatic model classification of surfaces,[78] in zincblende systems only the (110) surface (see **Figure S4** of ESI) is non polar, whereas (111) and (100) are polar surfaces of type III. Polar surfaces are characterized by two not equivalent layers of opposite charged ions that alternate along the normal to the surface; each repeat unit bears a dipole moment that increases with the number of the layers and determines the larger instability of these surfaces. Considering the large difference in E_S between polar and non polar surfaces, polar ones are not likely to be exposed at the ZnS nanoparticles to a sizable extent, even if, several electronic and structural reconstruction can contribute to a significant stabilization of such surfaces.[79] Therefore, in the present work, the interaction with CO has been studied only considering the most stable non polar (110) surface. At this surface, the ions of each specie are located along facing rows,

and each ion is coordinated by three neighbors instead of four as in the sphalerite bulk where every sulfur atom is tetrahedrally coordinated by four zinc atoms and vice versa.

The geometrical structure of the (110) surface is sketched in **Figure 4**. The top ZnS layer appears corrugated with respect to the bulk termination (see also Figure S4 of ESI). Indeed comparing the spacing between ZnS layers in the bulk (3.86 Å), Zn and S ions in the outermost layer are respectively downshifted by 0.368 Å and upshifted by 0.104 Å; the result is that the Zn ions become almost coplanar with respect to the adjacent S atoms with Zn-S distances that are considerably shorter (2.280 and 2.308 Å, see **Figure 4**) with respect to the corresponding values in the inner layers (2.360 Å).

The main features of the CO/ZnS interaction are reported in **Table 2** and the adsorption configurations schematically reported in **Figure 5**. The effect of the coverage on the adsorption properties was also analyzed; in all cases, CO interacts through the C atom with the Zn cations, *i.e.* with the Lewis acid centres of the surface. We first consider the low coverage case (θ=0.5). The most relevant geometrical feature is the slight shortening of the C-O distance (by 0.004 Å) with respect to the gas phase molecule and an upshift of the Zn cation bound to CO of about 0.15 Å. The adsorption energy ΔE_{ads} =-0.24 eV, is rather weak in line with the experimental observation that CO adducts are not stable at RT. The computed CO stretching mode, ν(C-O)=2182 cm^{-1} is blue shifted by 40 cm^{-1} with respect to the gas phase molecule, in excellent agreement with FTIR data, see **Figure 3**, and consistent with the shortening of the bond distance upon adsorption.

The interaction between CO and oxides surfaces has been widely investigated.[25] It is possible to distinguish between two mechanisms depending on the surface cation the CO is interacting with. If the cation has no d-electrons or a closed d shell, the interaction is mainly due to electrostatic effects[25,76] with sometimes a small amount of σ donation due to the overlap of the CO HOMO (a filled σ - "lone pair" orbital located on the C atom) with empty metal orbitals. In this case a shortening of the CO bond length and consequent blue shift of the CO vibrational frequency is reported. If the cation has d-electrons, the main contribution to the ΔE_{ads} is a due to a back donation mechanism. This is a π bonding interaction due to overlap of filled metal dπ orbitals with the LUMO of the CO molecule. Since electron density is introduced into a CO antibonding orbital there is a consequent elongation in the CO bond length and a red shift is observed in the IR spectra.

The electron structure at the CO/ZnS interface can be elucidated by considering the projected density of states PDOSs reported in Figure 6. Inspection of the figure shows that: i) the top of ZnS valence band is dominated by the 3sp states of S with small contribution from 4sp Zn states; the closed 3d Zn shell is much lower in energy (about 12 eV below the Fermi level E_f,); ii) the molecular orbitals of CO are rigidly downshifted upon interaction with the surface; iii) the 5σ

appears slightly widened and overlaps the bottom of the ZnS conduction band, that is with Zn 4sp empty states; iv) ZnS/CO Fermi level E_f upshifts by 0.7 eV with respect to bare ZnS. These features are in agreement with an interaction mechanism mainly of electrostatic nature but with a not negligible amount of σ donation from the non bonding filled 5σ of CO to ZnS. The absence of the retrodonation from surface zinc atoms is confirmed by several other theoretical works related to carbon monoxide adsorption over ZnO surfaces,[80-82] and on many other transition metal oxides such as TiO_2, etc.[26,83]

Moving to high coverage (θ=1.0) the adsorption energies ΔE_{ads} =-0.21 kcal mol^{-1} decrease by 0.04 eV concomitantly to a longer C-Zn distance by 0.035 Å with respect the θ=0.5 case. The vibrational frequency decreases, Δν(C-O)= 29 cm^{-1}, and is indeed red shifted by 23 cm^{-1} with respect to the low coverage case owing to the dipole -dipole interaction between CO molecules located at a short distance (3.850Å), **Table 2**.

Discussion and Conclusions

The surface properties of nanostructured ZnS materials have been studied by a combined experimental and computational approach. ZnS nanoparticles have been prepared by an easy precipitation method and activated in vacuum in order to clean the surface without affecting the stability of the cubic ZnS phase. This resulted in a series of samples with increasing particle size and crystallinity, as documented by XRD and HRTEM analyses. The surface properties of the ZnS nanoparticles have been investigated by employing the CO probe molecule. The results have been also compared to those of a commercial bulk ZnS sample (particle size < 10 μm). A small amount of ZnO and hexagonal ZnS phases formed by high temperature treatment have been not considered to be significant for data interpretation.

CO adsorption experiments have been followed by FTIR spectroscopy. Experiments showed the formation of a single CO peak that shifts to lower frequency with coverage increase, as a consequence of CO dipole-dipole lateral interactions. Interestingly, the position of CO band at low coverage has been found to be dependent on the ZnS particle size, in that it moves to lower frequency while particle size increases. In particular ν(C-O) moves from 2191 cm^{-1} in ZnS sample activated at 673 K, to 2185 cm^{-1} in the one treated at 973K, to 2175 cm^{-1} in bulk ZnS. This feature can thus be taken as an indication of ZnS nanostructuration.

Adsorption properties have been modeled by considering the interaction of CO with the ZnS (110) surface. Such surface is largely the most stable one, the only non polar one among the low index surfaces, and the only one expected to be exposed in a microcrystal.[39-41] Computed frequencies are in excellent agreement with the experimental spectrum. It is evident looking at

Figure 3b where the computed CO vibration frequencies are overlapped to the experimental spectra. The ν(C-O) blue shift and the concomitantly slight shortening of the bond distance in the adsorbed molecule are the result of interaction mechanism at the CO/ZnS interface, mainly of electrostatic nature but with a not negligible amount of σ donation. The adsorption energy, ΔE_{ads} =-0.24 eV (θ=0.5) is much weaker with respect to ZnO, ΔE_{ads} =-0.56 eV,[63] in very good agreement with the observation that, unlike ZnO, no CO adducts are formed at RT on ZnS nanoparticles.

To summarize, in this work on the basis of the experimental and computational results we have demonstrated that:

i) the (110) surface is the only one experienced by CO. The other surfaces may be present but not available for the interaction in reasons of reconstruction mechanisms or of a very low concentration.

ii) the strength of Zn^{2+} Lewis acidity in ZnS is considerably lower than in ZnO and more comparable to those of other oxides like TiO_2 (ΔE_{ads} =-0.22 eV) and MgO (ΔE_{ads} =-0.11 eV).[21,65]

iii) the surface Lewis acidity of Zn^{2+} sites in ZnS nanocrystals appears significantly different with respect to the same sites in microcrystals.

Acknowledgments

Italian Ministry for Research and University (MIUR) is gratefully acknowledged for funding project PRIN 2009BLNJC5 “Optimization of the photothermocatalytic sulfur-ammonia process for hydrogen production.” We thank Dr Patrizia Davit for kind help and fruitful discussion.

Table 1. General properties of the ZnS sample as a function of thermal activation in vacuum

Sample treatment	Crystallite size (nm)		SSA [b] (m^2/g)	Pore volume (cm^3/g)[c]	Pore width (Å)[c]
	XRD [a]	TEM			
As such	2.0	2.6 ± 0.4	376	0.60	25
673 K	3.7	4.9 ± 2.3	123	0.25	46
773 K	4.5	6.4 ± 1.0	70	0.22	75
973 K	23.8	35.0 ± 6.1	29	0.29	1000

[a] Calculated with the Scherrer equation; [b] measured by BET equation; [c] measured by BJH method in the isotherm adsorption branch.

Table 2. Main features of the CO interaction with the ZnS (110) surface at different CO coverage **θ**; d are the bond distances in Å, d_x and d_y are the shortest distances between C of adsorbed CO along the x and y direction (see Figure 5); ν(C-O) is the CO stretching frequency and Δν are the absolute differences with respect to the free molecule, in cm^{-1}; in parentheses the corresponding intensity in km mol^{-1}. In order to facilitate comparison with experiments, frequencies have been scaled by a factor f=0.9588. ΔE_{ads} is the BSSE corrected adsorption energy and it is reported in eV.

	θ=0.5	**θ=1.0**
d(C-O)[1]	1.119	1.120
d(C-Zn)	2.307	2.346
d_y(C-C)	7.700	3.850
d_x(C-C)	5.456	5.456
ΔE_{ads}	-0.244	-0.207
ν(C-O)	2182 (64)	2172 (116)
Δν(C-O)	39	29

[1] Computed CO gas phase properties: d(C-O)=1.125 Å, ν(C-O)=2143 cm^{-1}

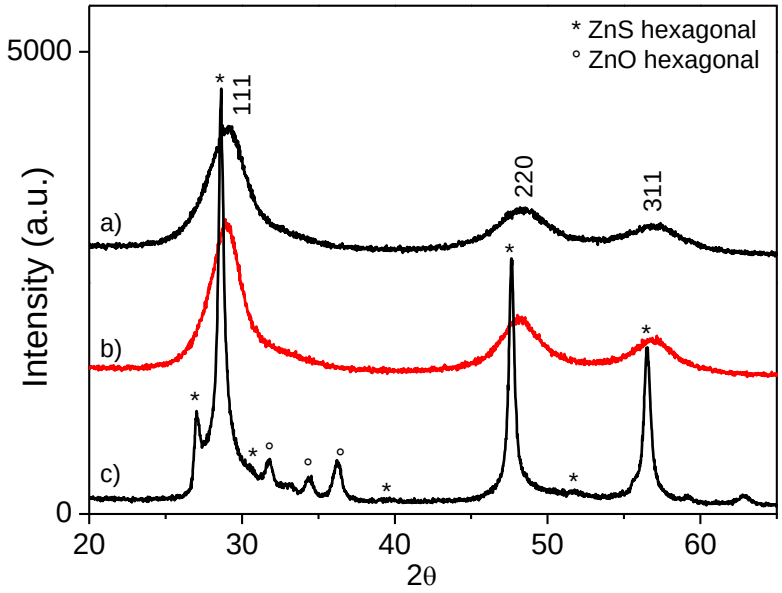

Figure 1. XRD patterns of ZnS particles activated in vacuum at a) 673 K, b) 773 K and c) 973 K. Labeled peaks correspond to the cubic sphalerite structure; * and ° peaks are due to the hexagonal ZnS and ZnO structures, respectively. Curves were vertically shifted for easier comparison.

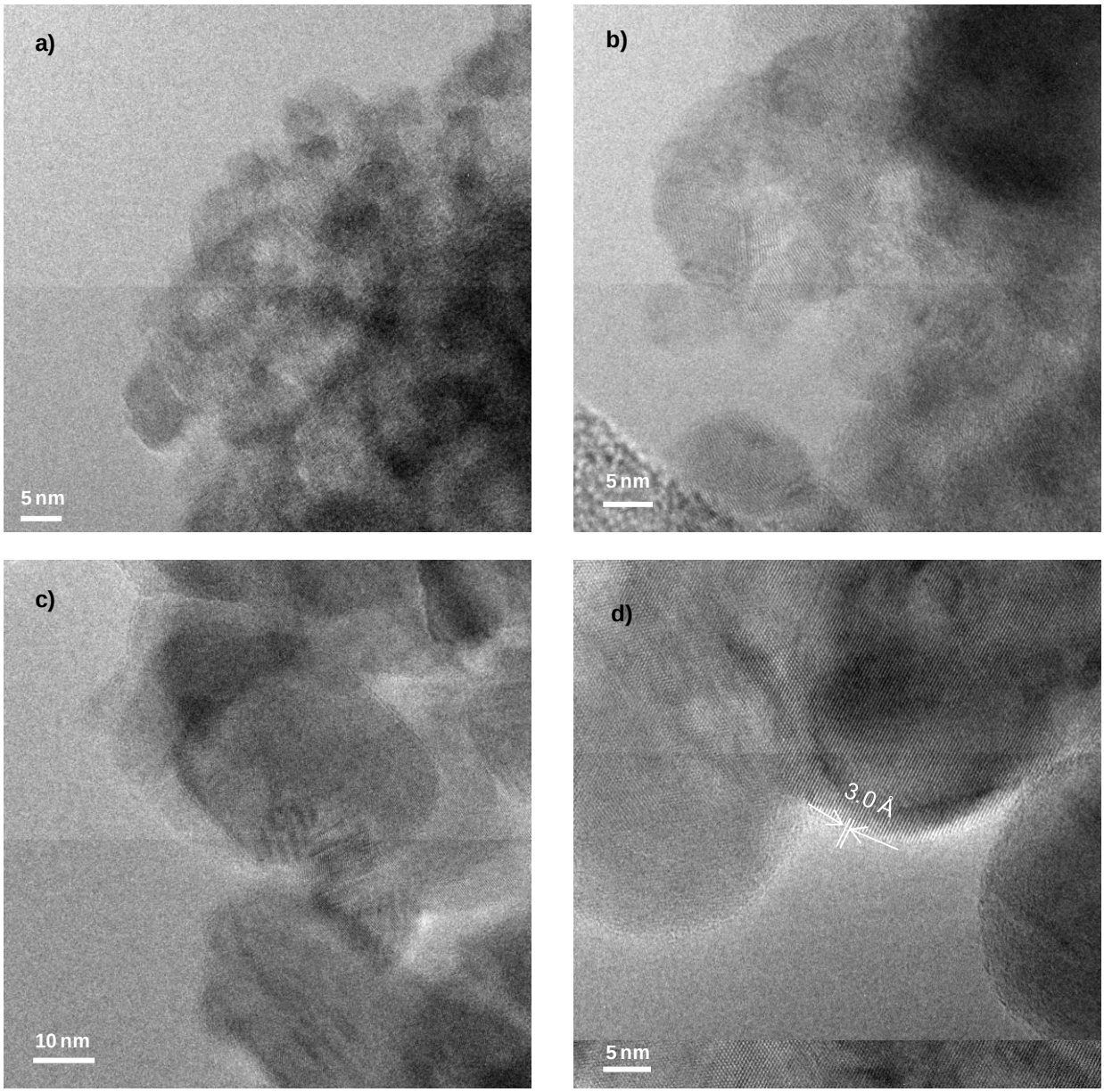

Figure 2. TEM images of the synthesized ZnS samples activated in vacuum at a) 673 K (300,000 X), b) 773 K (400,000 X) and c) 973 K (250,000 X); d) bulk ZnS (400,000 X).

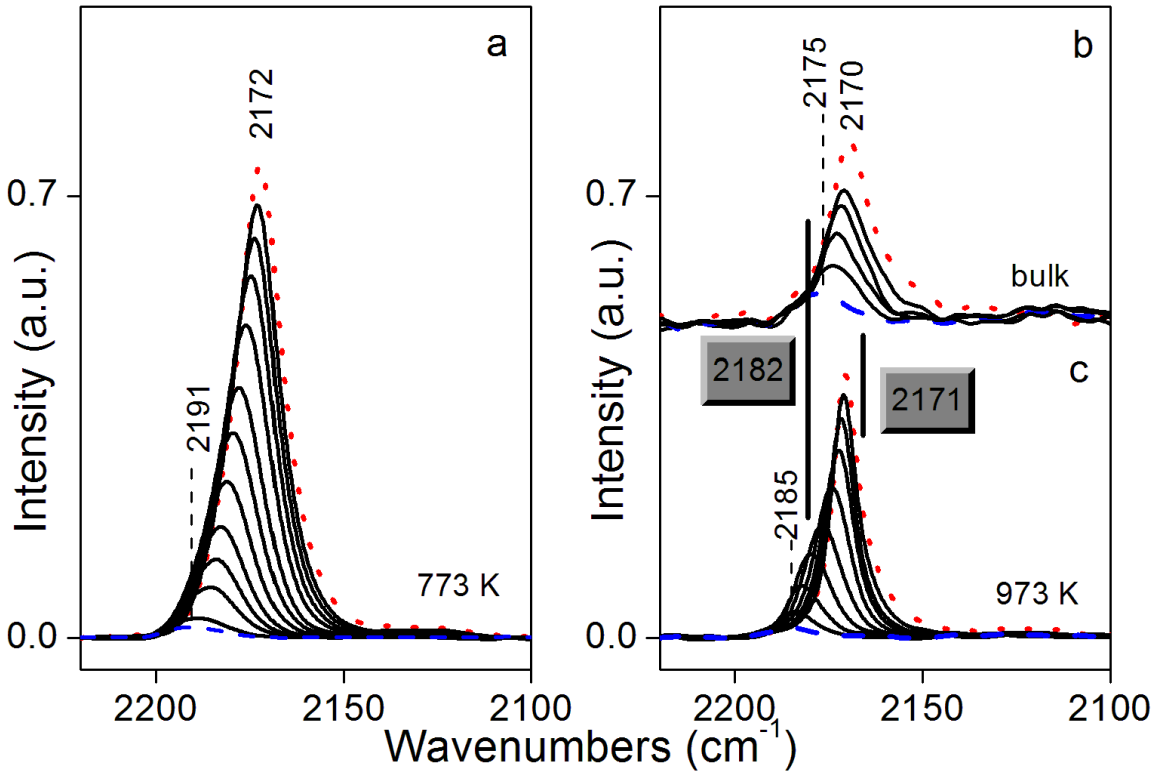

Figure 3. FTIR spectra of CO (decreasing pressure from 2.7 to 1 10-3 mbar) adsorbed at 110 K on the ZnS sample activated in vacuum at a) 673 and b) 973 K. Same spectra obtained on bulk ZnS activated at 673 K are reported in panel b, vertically translated for comparison. Computed frequencies at θ=0.5 and θ=1 are indicated in gray boxes and bold lines in panel b).

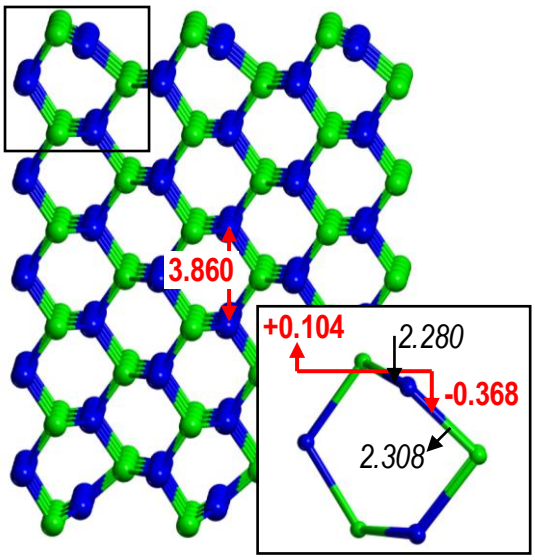

Figure 4. Side view of the 110 surface upon geometry relaxation. In the insert: zinc cations (blue spheres) and sulfur anions (green spheres); plane displacement in red; ZnS distances in black.

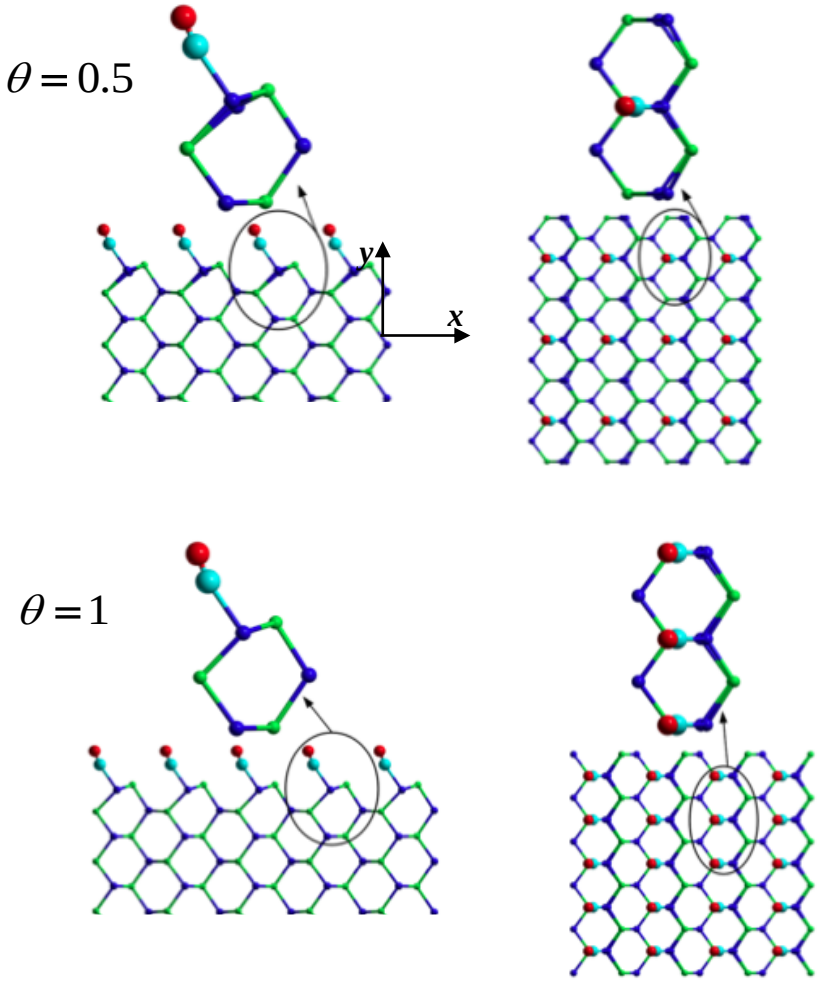

Figure 5. Geometry of the interaction between CO and the ZnS (110) surface. The two coverage degrees are reported. Side views on left panels, top views on right panels.

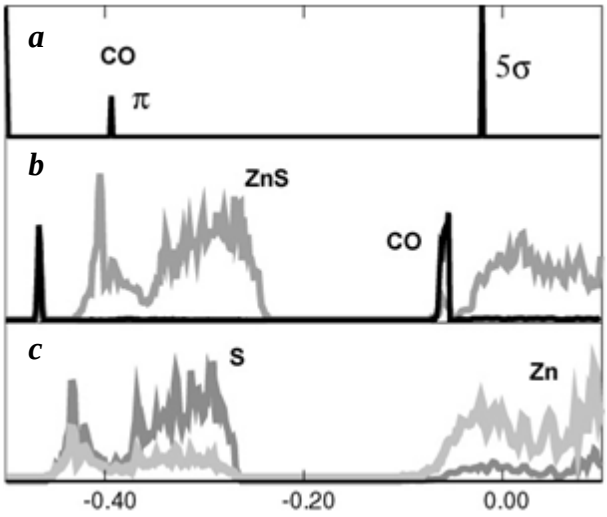

Figure 6. Projected density of states: a) CO free; c) free ZnS (110) projections on Zn and S states; b) ZnS/CO projections on ZnS and CO states. Energy in hartree. The Fermi level has been located in correspondence of the top of the VB.

References

(1) Fang, X. S.; Bando, Y.; Gautam, U. K.; Zhai, T. Y.; Zeng, H. B.; Xu, X. J.; Liao, M. Y.; Golberg, D. ZnO and ZnS Nanostructures: Ultraviolet-Light Emitters, Lasers, and Sensors. *Crit. Rev. Solid State Mater. Sci*. **2009**, *34*, 190-223.

(2) Fang, X. S.; Bando, Y.; Liao, M. Y.; Gautam, U. K.; Zhi, C. Y.; Dierre, B.; Liu, B. D.; Zhai, T. Y.; Sekiguchi, T.; Koide, Y.; Golberg, D. Single-Crystalline ZnS Nanobelts as Ultraviolet-Light Sensors. *Adv. Mater.* **2009**, *21*, 2034-2039.

(3) Liu, H.; Hu, L.; Watanabe, K.; Hu, X.; Dierre, B.; Kim, B.; Sekiguchi, T.; Fang, X. Cathodoluminescence Modulation of ZnS Nanostructures by Morphology, Doping, and Temperature. *Adv. Funct. Mater*. **2013**, *23*, 3701-3709.

(4) Pan, D.; Weng, D.; Wang, X.; Xiao, Q.; Chen, W.; Xu, C.; Yang, Z.; Lu, Y. Alloyed semiconductor nanocrystals with broad tunable band gaps. *Chem. Commun.* **2009**, 4221-4223.

(5) Celikkaya, A.; Mufit, A. Preparation and mechanism of formation of spherical submicrometer zinc sulfide powders. *J. Am. Ceram. Soc.* **1990**, *65*, 2360-2365.

(6) Kanemoto, M.; Hosokawa, H.; Wada, Y.; Murakoshi, K.; Yanagida, S.; Sakata, T.; Mori, H.; Ishikawa, M.; Kobayashi, H. Semiconductor photocatalysis .20. Role of surface in the photoreduction of carbon dioxide catalysed by colloidal ZnS nanocrystallites in organic solvent. *J. Chem. Soc., Faraday Trans.* **1996**, *92*, 2401-2411.

(7) Yu, S.-h. Optical properties of ZnS nanosheets , ZnO dendrites , and their lamellar precursor ZnS. *Chem. Phys. Lett.* **2002**, *361*, 362-366.

(8) Nakaoka, Y.; Nosaka, Y. Electron spin resonance study of radicals produced by photoirradiation on quantized and bulk ZnS particles. *Langmuir* **1997**, *13*, 708-713.

(9) Fang, X. S.; Ye, C. H.; Zhang, L. D.; Wang, Y. H.; Wu, Y. C. Temperature-controlled catalytic growth of ZnS nanostructures by the evaporation of ZnS nanopowders. *Adv. Funct. Mater.* **2005**, *15*, 63-68.

(10) Fang, X.; Bando, Y.; Ye, C.; Shen, G.; Golberg, D. Shape- and size-controlled growth of ZnS nanostructures. *J. Phys. Chem. C* **2007**, *111*, 8469-8474.

(11) Fang, X.; Bando, Y.; Liao, M.; Zhai, T.; Gautam, U. K.; Li, L.; Koide, Y.; Golberg, D. An Efficient Way to Assemble ZnS Nanobelts as Ultraviolet-Light Sensors with Enhanced Photocurrent and Stability. *Adv. Funct. Mater.* **2010**, *20*, 500-508.

(12) Al-Rasoul, K. T.; Abbas, N. K.; Shanan, Z. J. Structural and Optical Characterization of Cu and Ni Doped ZnS Nanoparticles. *Int. J. Electrochem. Sci.* **2013**, *8*, 5594-5604.

(13) Arai, T.; Senda, S.-i.; Sato, Y.; Takahashi, H.; Shinoda, K.; Jeyadevan, B.; Tohji, K. Cu-doped ZnS hollow particle with high activity for hydrogen generation from alkaline sulfide solution under visible light. *Chem. Mater.* **2008**, *20*, 1997-2000.

(14) Borse, P. H.; Srinivas, D.; Shinde, R. F.; Date, S. K.; Vogel, W.; Kulkarni, S. K. Effect of Mn2+ concentration in ZnS nanoparticles on photoluminescence and electron-spin-resonance spectra. *Phys. Rev. B* **1999**, *60*, 8659-8664.

(15) Car, B.; Medling, S.; Corrado, C.; Bridges, F.; Zhang, J. Z. Probing the local structure of dilute Cu dopants in fluorescent ZnS nanocrystals using EXAFS. *Nanoscale* **2011**, *3*, 4182-4189.

(16) Kudo, A.; Niishiro, R.; Iwase, A.; Kato, H. Effects of doping of metal cations on morphology, activity, and visible light response of photocatalysts. *Chem. Phys.* **2007**, *339*, 104-110.

(17) Nag, A.; Sapra, S.; Nagamani, C.; Sharma, A.; Pradhan, N.; Bhat, S. V.; Sarma, D. D. A study of Mn2+ doping in CdS nanocrystals. *Chem. Mater.* **2007**, *19*, 3252-3259.

(18) Norris, D. J.; Efros, A. L.; Erwin, S. C. Doped nanocrystals. *Science* **2008**, *319*, 1776-1779.

(19) Sarkar, S.; Guria, A. K.; Pradhan, N. Influence of doping on semiconductor nanocrystals mediated charge transfer and photocatalytic organic reaction. *Chem. Commun.* **2013**, *49*, 6018-6020.

(20) Kudo, A.; Kato, H.; Tsuji, I. Strategies for the development of visible-light-driven photocatalysts for water splitting. *Chem. Lett.* **2004**, *33*, 1534-1539.

(21) Gilbert, B.; Huang, F.; Lin, Z.; Goodell, C.; Zhang, H. Z.; Banfield, J. F. Surface chemistry controls crystallinity of ZnS nanoparticles. *Nano Lett.* **2006**, *6*, 605-610.

(22) Rajh, T.; Chen, L. X.; Lukas, K.; Liu, T.; Thurnauer, M. C.; Tiede, D. M. Surface restructuring of nanoparticles: An efficient route for ligand-metal oxide crosstalk. *J. Phys. Chem. B* **2002**, *106*, 10543-10552.

(23) Zhang, H. Z.; Gilbert, B.; Huang, F.; Banfield, J. F. Water-driven structure transformation in nanoparticles at room temperature. *Nature* **2003**, *424*, 1025-1029.

(24) Goodell, C. M.; Gilbert, B.; Weigand, S. J.; Banfleld, J. F. Kinetics of water adsorption-driven structural transformation of ZnS nanoparticles. *J. Phys. Chem. C* **2008**, *112*, 4791-4796.

(25) Lamberti, C.; Zecchina, A.; Groppo, E.; Bordiga, S. Probing the surfaces of heterogeneous catalysts by in situ IR spectroscopy. *Chem. Soc. Rev.* **2010**, *39*, 4951-5001.

(26) Mino, L.; Ferrari, A. M.; Lacivita, V.; Spoto, G.; Bordiga, S.; Zecchina, A. CO Adsorption on Anatase Nanocrystals: A Combined Experimental and Periodic DFT Study. *J. Phys. Chem. C* **2011**, *115*, 7694-7700.

(27) Müller, B.; van Langeveld, A. D.; Moulijn, J. A.; Knözinger, H. Characterization of sulfided molybdenum/alumina catalysts by temperature-programmed reduction and low-temperature Fourier transform infrared spectroscopy of adsorbed carbon monoxide. *J. Phys. Chem.* **1993**, *97*, 9028-9033.

(28) Mauge, F.; Lamotte, J.; Nesterenko, N. S.; Manoilova, O.; Tsyganenko, A. A. FT-IR study of surface properties of unsupported MoS2. *Catal. Today* **2001**, *70*, 271-284.

(29) Tsyganenko, A. A.; Can, F.; Travert, A.; Maugé, F. FTIR study of unsupported molybdenum sulfide — in situ synthesis and surface properties characterization. *Appl. Catal. A Gen.* **2004**, *268*, 189-197.

(30) Cesano, F.; Bertarione, S.; Piovano, A.; Agostini, G.; Rahman, M. M.; Groppo, E.; Bonino, F.; Scarano, D.; Lamberti, C.; Bordiga, S.; Montanari, L.; Bonoldi, L.; Millini, R.; Zecchina, A. Model oxide supported MoS2 HDS catalysts: structure and surface properties. *Catal. Sci. Technol.* **2011**, *1*, 123-136.

(31) Lubezky, A.; Folman, M. IR spectra of CO adsorbed on Si, Ge and ZnS evaporated films. *J. Chem. Soc., Faraday Trans. 1* **1981**, *77*, 791-796.

(32) Hertl, W. SURFACE CHEMICAL-PROPERTIES OF ZINC-SULFIDE. *Langmuir* **1988**, *4*, 594-598.

(33) Yamamoto, T.; Taniguchi, A. ZNS DOPED BY ELECTRON DONATING ORGANIC LIGAND (L = BPY, PHEN, PY) AND CONTROL OF SEMICONDUCTING PROPERTIES OF ZNS BY THE LIGAND. *Inorg. Chim. Acta* **1985**, *97*, L11-L13.

(34) Cooper, J. K.; Franco, A. M.; Gul, S.; Corrado, C.; Zhang, J. Z. Characterization of Primary Amine Capped CdSe, ZnSe, and ZnS Quantum Dots by FT-IR: Determination of Surface Bonding Interaction and Identification of Selective Desorption. *Langmuir* **2011**, *27*, 8486-8493.

(35) Scholz, S. M.; Vacassy, R.; Lemaire, L.; Dutta, J.; Hofmann, H. Nanoporous aggregates of ZnS nanocrystallites. *Appl. Organomet. Chem.* **1998**, *12*, 327-335.

(36) Murugadoss, G. Synthesis, optical, structural and thermal characterization of Mn2+ doped ZnS nanoparticles using reverse micelle method. *J. Lumin.* **2011**, *131*, 2216-2223.

(37) Zhang, H. Z.; Chen, B.; Gilbert, B.; Banfield, J. F. Kinetically controlled formation of a novel nanoparticulate ZnS with mixed cubic and hexagonal stacking. *J. Mater. Chem.* **2006**, *16*, 249-254.

(38) Wang, L.; Zhao, C.; Meng, F.; Huang, S.; Yuan, X.; Xu, X.; Yang, Z.; Yang, H. Optical properties and simultaneous synthesis of ZnS and ZnO nanoparticles via one reverse micellar system. *Colloid Surf. A* **2010**, *360*, 205-209.

(39) Emin, S.; Lisjak, D.; Pitcher, M.; Valant, M. Structural and morphological transformations of textural porous zinc sulfide microspheres. *Microporous Mesoporous Mater.* **2013**, *165*, 185-192.

(40) Siriwardane, R. V.; Woodruff, S. In situ Fourier transform infrared characterization of sulfur species resulting from the reaction of water vapor and oxygen with zinc sulfide. *Ind. Eng. Chem. Res.* **1997**, *36*, 5277-5281.

(41) Savic, T. D.; Saponjic, Z. V.; Comor, M. I.; Nedeljkovic, J. M.; Dramicanin, M. D.; Nikolic, M. G.; Veljkovic, D. Z.; Zaric, S. D.; Jankovic, I. A. Surface modification of anatase nanoparticles with fused ring salicylate-type ligands (3-hydroxy-2-naphthoic acids): a combined DFT and experimental study of optical properties. *Nanoscale* **2013**, *5*, 7601-7612.

(42) Yang, J.; Xue, C.; Yu, S.-H.; Zeng, J.-H.; Qian, Y.-T. General Synthesis of Semiconductor Chalcogenide Nanorods by Using the Monodentate Ligand n-Butylamine as a Shape Controller. *Angew. Chem. Int. Ed.* **2002**, *41*, 4697-4700.

(43) Murakoshi, K.; Hosokawa, H.; Tanaka, N.; Saito, M.; Wada, Y.; Sakata, T.; Mori, H.; Yanagida, S. Phase transition of ZnS nanocrystallites induced by surface modification at ambient temperature and pressure confirmed by electron diffraction. *Chem. Commun.* **1998**, 321-322.

(44) Berlier, G.; Meneau, F.; Sankar, G.; Catlow, C. R. A.; Thomas, J. M.; Spliethoff, B.; Schueth, F.; Coluccia, S. Synthesis and characterisation of small ZnS particles. *Res. Chem. Intermed.* **2006**, *32*, 683-693.

(45) Sajadi, M. S.; Pourahmad, A.; Sohrabnezhad, S.; Zare, S. Formation of NiS and CoS Semiconductor Nanoparticles Inside Mordenite-Type Zeolite. *Mater. Lett.* **2007**, *61*, 2923-2926.

(46) Lindroos, S.; Charreire, Y.; Bonnin, D.; Leskela, M. Growth and characterization of zinc sulfide thin films deposited by the successive ionic layer adsorption and reaction (silar) method using complexed zinc ions as the cation precursor. *Mater. Res. Bull.* **1998**, *33*, 453-459.

(47) Hamad, S.; Catlow, C. R. A.; Spano, E.; Matxain, J. M.; Ugalde, J. M. Structure and properties of ZnS nanoclusters. *J. Phys. Chem. B* **2005**, *109*, 2703-2709.

(48) Hamad, S.; Cristol, S.; Catlow, C. R. A. Simulation of the embryonic stage of ZnS formation from aqueous solution. *J. Am. Chem. Soc.* **2005**, *127*, 2580-2590.

(49) Hamad, S.; Catlow, C. R. A. Computational study of the relative stabilities of ZnS clusters, for sizes between 1 and 4 nm. *J. Cryst. Growth* **2006**, *294*, 2-8.

(50) Hamad, S.; Woodley, S. M.; Catlow, C. R. A. Experimental and computational studies of ZnS nanostructures. *Mol. Simul.* **2009**, *35*, 1015-1032.

(51) Catlow, C. R. A.; Bromley, S. T.; Hamad, S.; Mora-Fonz, M.; Sokol, A. A.; Woodley, S. M. Modelling nano-clusters and nucleation. *Phys. Chem. Chem. Phys.* **2010**, *12*, 786-811.

(52) Sayle, D. C.; Mangili, B. C.; Klinowski, J.; Sayle, T. X. T. Simulating self-assembly of ZnS nanoparticles into mesoporous materials. *J. Am. Chem. Soc.* **2006**, *128*, 15283-15291.

(53) Matxain, J. M.; Eriksson, L. A.; Mercero, J. M.; Ugalde, J. M.; Spano, E.; Hamad, S.; Catlow, C. R. A. Electronic excitation energies of ZnS nanoparticles. *Nanotechnology* **2006**, *17*, 4100-4105.

(54) Zwijnenburg, M. A. Optical excitations in stoichiometric uncapped ZnS nanostructures. *Nanoscale* **2011**, *3*, 3780-3787.

(55) Zwijnenburg, M. A. Photoluminescence in semiconductor nanoparticles: an atomistic view of excited state relaxation in nanosized ZnS. *Nanoscale* **2012**, *4*, 3711-3717.

(56) Zwijnenburg, M. A. Excited state localisation cascades in inorganic semiconductor nanoparticles. *Phys. Chem. Chem. Phys.* **2013**, *15*, 11119-11127.

(57) Zwijnenburg, M. A.; Illas, F.; Bromley, S. T. The fate of optical excitations in small hydrated ZnS clusters: a theoretical study into the effect of hydration on the excitation and localisation of electrons in Zn4S4 and Zn6S6. *Phys. Chem. Chem. Phys.* **2011**, *13*, 9311-9317.

(58) Azpiroz, J. M.; Mosconi, E.; Ugalde, J. M.; De Angelis, F. Effect of Structural Dynamics on the Opto-Electronic Properties of Bare and Hydrated ZnS QDs. *J. Phys. Chem. C* **2014**, *118*, 3274-3284.

(59) Sun, W.; Corni, S.; Di Felice, R. Reactivity of the ZnS (1010) Surface to Small Organic Ligands by Density Functional Theory. *J. Phys. Chem. C* **2013**, *117*, 16034-16041.

(60) Brunauer, S.; Emmet, P. H.; Teller, E. Adsorption of Gases in Multimolecular Layers. *J. Am. Chem. Soc.* **1938**, *60*, 309-319.

(61) Webb, P. A.; Orr, C., *Analytical Methods in Fine Particle Technology*; Micromeritics Instrument Corp.: Norcross, GA, USA, **1997**.

(62) Barret, E. P.; Joyner, L. G.; Halenda, P. P. The Determination of Pore Volume and Area Distributions in Porous Substances. I. Computations from Nitrogen Isotherms. *J. Am. Chem. Soc.* **1951**, *73*, 373–380.

(63) Pierce, C. Computation of Pore Sizes from Physical Adsorption Data. *J. Phys. Chem.* **1953**, *57*, 149-152.

(64) CRYSTAL09 User's Manual 2009, University of Torino.

(65) Adamo, C.; Barone, V. *J. Chem. Phys.* **1999**, *110*, 6158-6170.

(66) Basis set exchange https://bse.pnl.gov/bse/portal.

(67) Stevens, W. J.; Krauss, M.; Bash, H.; Jaisen, P. G. *Can. J. Chem.* **1992**, *70*, 612-630.

(68) www.crystal.unito.it.

(69) Boys, S. F.; Bernardi, F. The calculation of small molecular interaction by the difference of separate total energies. Some procedures with reduced errors. *Mol. Phys.* **1970**, *19*, 553-566.

(70) Yeh, C. Y.; Lu, Z. W.; Froyen, S.; Zunger, A. Zinc-Blende-Wurtzite Polytypism in Semiconductors. *Phys. Rev. B* **1992**, *46*, 10086-10097.

(71) Fang, X.; Zhai, T.; Gautam, U. K.; Li, L.; Wu, L.; Bando, Y.; Golberg, D. ZnS nanostructures: From synthesis to applications. *Prog. Mater Sci.* **2011**, *56*, 175-287.

(72) Qadri, S. B.; Skelton, E. F.; Hsu, D.; Dinsmore, A. D.; Yang, J.; Gray, H. F.; Ratna, B. R. Size-induced transition-temperature reduction in nanoparticles of ZnS. *Phys. Rev. B* **1999**, *60*, 9191-9193.

(73) Akiyama, T.; Sano, K.; Nakamura, K.; Ito, T. An empirical interatomic potential approach to structural stability of ZnS and ZnSe nanowires. *Jpn. J. Appl. Phys., Part 1* **2007**, *46*, 1783-1787.

(74) Zhang, X. F.; Sun, Z. H.; Yan, W. S.; Wei, F.; Wei, S. Q. Structural evolutions of CdSe nanocrystals in ripening process. *Mater. Chem. Phys.* **2008**, *111*, 513-516.

(75) Rockenberger, J.; Troger, L.; Kornowski, A.; Vossmeyer, T.; Eychmuller, A.; Feldhaus, J.; Weller, H. EXAFS studies on the size dependence of structural and dynamic properties of CdS nanoparticles. *J. Phys. Chem. B* **1997**, *101*, 2691-2701.

(76) Scarano, D.; Spoto, G.; Bordiga, S.; Zecchina, A.; Lamberti, C. Lateral interactions in CO adlayers on prismatic ZnO faces: a FTIR and HRTEM study. *Surf. Sci.* **1992**, *276*, 281-298.

(77) Ghiotti, G.; Boccuzzi, F.; Scala, R. INFRARED STUDY OF ZNO SURFACE-PROPERTIES - CO ADSORPTION AND CO/D2 INTERACTION AT 77-K. *J. Catal.* **1985**, *92*, 79-97.

(78) Tasker, P. W. *J. Phys. Chem.* **1979**, *12*, 4977.

(79) Goniakowski, J.; Finocchi, F.; Noguera, C. Polarity of oxide surfaces and nanostructures. *Rep. Prog. Phys.* **2008**, *71*.

(80) Lopes Martins, J. B.; Longo, E.; Roriguez Salmon, O. D.; Espinoza, V. A. A.; Taft, C. A. The interaction of H2, CO, CO2, H2O and NH3 on ZnO surfaces: an oniom study. *Chem. Phys. Lett.* **2004**, *400*, 481 – 486.

(81) Casarin, M.; Maccato, C.; Vittadini, A. Theoretical Investigation of the Chemisorption of H2 and CO on the ZnO (1010) surface. *Inorg. Chem.* **1998**, *37*, 5482-5490.

(82) Jaffe, E.; Hess, A. C. Ab initio study of a CO monolayer adsorbed on the (1010) surface of ZnO. *J. Chem. Phys.* **1996**, *104*, 3348– 3351.

(83) Ugliengo, P.; Damin, A. Are dispersive forces relevant for CO adsorption at the MgO(100) surface? *Chem. Phys. Lett.*, **2002**, *366*, 683-690.

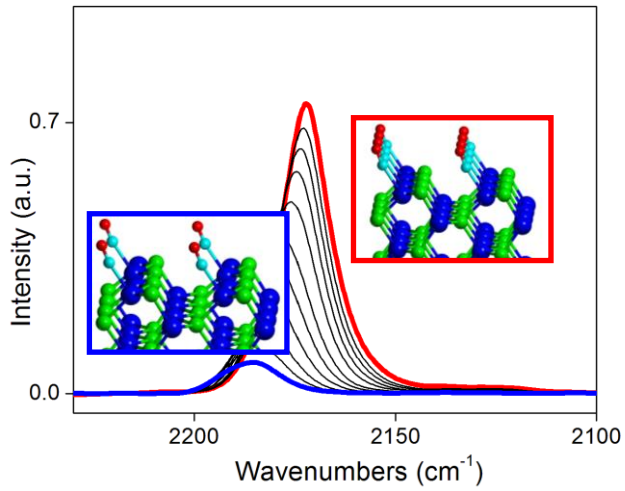

Graphical abstract